Measurements and modeling of nonlocal resistance in the fractional quantum Hall effect

J. K. Wang and V. J. Goldman
Department of Physics, State University of New York, Stony Brook, New York 11794-3800
(Received 5 December 1991)

Recently, we have reported the observation of nonlocal resistance in the regime of the fractional quantum Hall effect (FQHE) that clearly demonstrates edge-state conduction over macroscopic distances. In this paper we present measurements of nonlocal resistance with variations of sample geometry, magnetic-field direction, temperature, and applied current. From our results we formulate a picture of transport in the FQHE regime via coexisting edge and bulk states. Scattering of edge currents is largely suppressed over distances of ~ 1 mm at low temperatures. Edge currents are partially redistributed into the bulk at Ohmic contacts on the sample periphery. This results in potential drops between Ohmic contacts far from the bulk-only current path, i.e., nonlocal resistances. For analysis of our data, we introduce a FQHE extension of the bulk-edge transport model successfully applied by Szafer *et al.* in the integer QHE regime. We discuss the current and temperature dependence of the data in terms of temperature-dependent scattering between edge and bulk currents, increasing with increasing current or temperature.

I. INTRODUCTION

The integer quantum Hall effect[1] (IQHE) can be understood in terms of transport by edge channels corresponding to an integer number of fully occupied Landau levels.[2-4] In this picture, near an integral Landau-level filling $\nu=i$, when the chemical potential μ lies in the localized bulk states, all current is carried by dissipationless edge channels and the Hall resistance is quantized to h/ie^2. Dissipative transport (between $\nu=i$ and $\nu=i+1$) occurs when current is carried both by extended bulk states of the partially occupied topmost Landau level and by the extended edge states. Much experimental research on edge-state transport has focused on two-dimensional electron systems (2DES) confined within narrow- and small-gated devices, where the effect of edge-state conduction is enhanced. Recent measurements[4] of nonlocal four-terminal magnetoresistance (FTMR) by McEuen *et al.* demonstrate dramatically, however, that edge-channel transport may be largely decoupled from the bulk over macroscopic distances of ~ 1 mm in 2DES samples exhibiting the IQHE.

Interpretation of the IQHE of noninteracting electrons in terms of edge channels is straightforward since for noninteracting electrons the edge channels are formed in one-to-one correspondence with the bulk Landau levels defined in the single-electron density of states.[2-4] The fractional quantum Hall effect[5] (FQHE) occurs at certain simple rational values of ν and is fundamentally an interacting-electron phenomenon. For $\nu=1/m$, where m is an odd integer, the FQHE states are very well described by the Laughlin many-electron incompressible states.[6] The rest of the FQHE states occur at $\nu=p/q$, where q is odd. These states, usually called "the hierarchy states," have been obtained in the Haldane-Halperin theory[7] and, more recently, in the Jain theory.[8] These theories[6-8] describe only bulk FQHE states, however.

Several theories of edge states in the FQHE regime have recently been proposed.[9-11] Chang and Cunningham[12] and Kouwenhoven *et al.*[13] have experimentally studied adiabatic edge-state transport in small gated samples; they discuss their results in terms of "edge channels" defined in the single-electron density of states. Chang and Cunningham performed measurements of a gate-induced "barrier" resistance on the $\nu=\frac{1}{3}$ and $\frac{2}{3}$ FQHE plateaus. Kouwenhoven *et al.* employed adjustable barriers as current and voltage probes and measured the Hall resistance. They interpreted their results in terms of selective population and detection of edge channels (three channels per Landau level, defined in the single-electron density of states) at $\nu=\frac{2}{3}$ and concluded that each such "edge channel" contributes a conductance of $e^2/3h$.

In an earlier Letter[14] we reported observation of nonlocal magnetotransport in ungated 2DES samples in the FQHE regime at arbitrary ν, demonstrating unambiguously (model-independently) edge-state conduction, decoupled from the bulk over macroscopic distances on the order of 1 mm. In this paper we present results from measurements of nonlocal resistances in the QHE regime upon variation of different experimental parameters. In Sec. II we outline a generalized picture of coexisting dissipative bulk and dissipationless edge conduction. First, we describe the one-parameter model applied by Szafer *et al.*[4] to bulk-edge transport in the IQHE. For comparison with our experimental results, we introduce an extension of this model to the FQHE regime. In Sec. III, following a brief description of materials and procedures, we present data illustrating the dependence of nonlocal resistances in the FQHE regime on sample geometry, magnetic-field (B) direction, temperature (T), B sweep direction, and applied dc current (I_{dc}). We analyze and discuss our results in Sec. IV. We deduce a picture of transport via coexisting bulk and edge states in the

FQHE, dependent upon overall sample geometry and the configuration of Ohmic contacts. We discuss the current and temperature dependence of the data in terms of T-dependent scattering between edge and bulk currents, increasing with increasing current or temperature. Final conclusions follow in Sec. V.

II. MODELING OF EDGE STATE TRANSPORT

In a 2DES, application of B perpendicular to the 2DES plane induces quantization of single-electron eigenenergies in discrete Landau levels. Disorder, inevitable in experimental systems, results in broadening of the Landau levels and localization of the single-electron states in the bulk of 2DES. In the IQHE regime,[1] the localization length diverges for bulk states at the centers of Landau levels;[2] a nonzero fraction of states in each Landau level is thus extended across a 2DES of finite size. In the limit of $T \rightarrow 0$, dissipative electron transport across the bulk 2DES can occur when these states are not completely occupied, that is, when the chemical potential μ lies in the extended bulk states.

In a 2DES of finite size, single-electron "edge" states are produced by the confining potential. For noninteracting electrons, quasi-one-dimensional edge-state channels are formed in one-to-one correspondence with the bulk Landau levels.[2] As shown in the energy diagram in Fig. 1, the confining potential raises the energy of the edge states above the corresponding centers of Landau levels in the bulk. One edge channel is occupied for each fully occupied Landau level. The edge states are all extended, even in the presence of moderate disorder, and carry current in one direction along the 2DES perimeter (lower plot, Fig. 1). A current $(\Delta\mu)(e^2/h)$ per occupied edge channel is carried by the edge states with energies within an interval $\Delta\mu$.[2] Backscattering of edge states is impossible; scattering into bulk states or across to the opposite edge is exponentially suppressed in macroscopic samples at low T; thus edge currents are dissipationless. Edge current originating from an Ohmic contact on the sample perimeter then depends only on the chemical potential μ at that contact. Current in the edge channels increases linearly with μ; one can introduce effective edge contact resistance of h/ie^2 when there are i occupied edge channels ($i < \nu < i+1$).

For measurements of 2DES transport, samples are commonly defined as a Hall bar pattern in the 2D plane, shown schematically in Fig. 2(a). Ohmic contacts to the 2DES are made at the six solid-line squares, labeled 1–6 inside the squares. We define $R_{ij,kl}$ as the FTMR measured as the potential difference between Ohmic contacts k and l, divided by current passed through Ohmic contacts i and j. That is, in discussing an FTMR $R_{ij,kl}$, we designate k and l as the voltage contacts, and i and j as the current contacts. Longitudinal FTMR, $R_{xx}(B)$, is measured as $R_{14,23}$ or $R_{14,65}$. Nonlocal FTMR, $R_{\rm NL}(B)$, is measured as $R_{26,35}$ or $R_{35,26}$, with current and voltage lead pairs at opposite ends of the Hall bar central segment [labeled "A" in Fig. 2(a)]. Nonzero R_{xx} implies dissipative conduction across the central segment. Nonzero $R_{\rm NL}$ implies that potential differences induced along edges extend largely unattenuated, i.e., edge currents are largely decoupled from the bulk, along the central segment.

McEuen *et al.* have recently reported FTMR measurements, using 2DES samples with Hall bar patterns.[4] Over different intervals of B in the IQHE regime, they

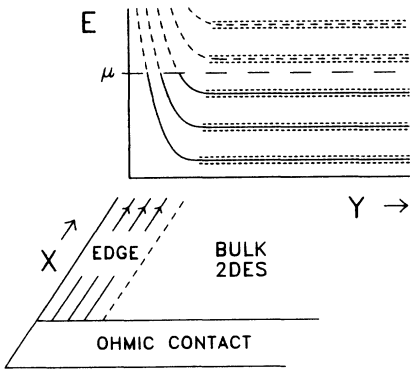

FIG. 1. Schematic diagrams of a 2DES in quantizing B, near the edge of its perimeter. Single-electron energy levels as a function of distance Y from the edge are shown in the upper plot. The solid curves represent three Landau levels and corresponding edge channels, filled up to chemical potential μ. The short-dashed horizontal lines represent broadening of bulk Landau levels by disorder. The lower plot (X vs Y) shows the 2DES plane. Edge current emerges from the Ohmic contact and travels in the direction determined by B.

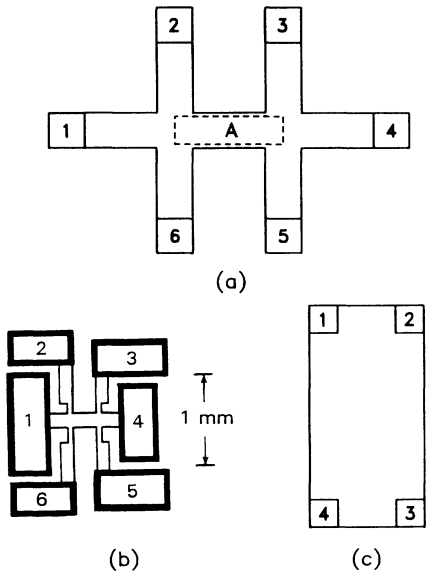

FIG. 2. Hall bar patterns. (a) Schematic: with six Ohmic contacts; the central segment is shown as the dashed-line rectangle in the center (labeled "A"); lead regions connect each of the contacts and the central segment. (b) Actual pattern defined on some of the samples with $L_A/W_A \approx 2.2$; $L_j/W_j \approx 5$–7 for the lead regions connecting to contacts 2, 3, 5, and 6. (c) A rectangular sample with four contacts.

observe $R_{NL}=0$ and $R_{xx}=0$, $R_{NL}\neq 0$ and $R_{xx}\neq 0$, and $R_{NL}=0$ and $R_{xx}\neq 0$. Data of the second type clearly demonstrate simultaneous dissipative bulk conduction and dissipationless edge conduction. They model FTMR's quantitatively, within the single-electron picture discussed above, for $i<\nu<i+1$. Dissipationless edge current circulates between Ohmic contacts in one direction around the sample perimeter.[15] Potential drops occur only as the edge current enters an Ohmic contact. On emerging from a contact, edge currents pass through a contact resistance h/ie^2. Additional current, subject to dissipation, circulates in parallel with the edge current, representing bulk conduction in the highest, partially filled Landau level. As modeled in Ref. 4, the bulk and edge currents flow independently in the 2DES, except in the sense that they emerge from each contact j at the same chemical potential μ_j. On emerging from a contact, the bulk current passes through a contact resistance of h/e^2. Dissipation in the 2DES interior is modeled in terms of partial reflection of the bulk current channel (to the opposite edge[16]) while circulating throughout the central segment and the lead regions of the Hall bar pattern. This reflection is parametrized in terms of a bulk resistivity scalar ρ. For the bulk current flowing through a lead region, e.g., in either direction between contact j and the central segment, transmission probability is

$$T_j=1/[1+\rho(e^2/h)(L_j/W_j)]\ , \tag{1}$$

where L_j and W_j are the length and width of the lead region to contact j. Due to the partial reflection, states in the bulk lead region j will be occupied up to a potential $\mu^B{}_j$, in general different from μ_j. $\mu^B{}_j$ is related to T_j and μ_j by imposing current conservation of bulk currents passing through lead region j between contact j and other bulk regions. In this model, the net total bulk and edge current emerging from contact j then is

$$I_j=(e^2/h)\{N_E(\mu_j-\mu_{j-1}) +N_B(\mu_j-\mu^B{}_j)[T_j/(1-T_j)]\}\ , \tag{2}$$

assuming that current channels circulate from contact 6 to 1 to 2 in Fig. 2(a). $N_E=i$ and $N_B=1$, corresponding to $i<\nu<i+1$. Variation of ρ from 0 to infinity corresponds to variation of ν from $i+1$ to i.

Nonzero nonlocal resistances can be explained qualitatively within this model. To measure $R_{26,35}$, for example, we pass current through contacts 2 and 6. Assuming that current channels circulate from contact 6 to 1 to 2, edge current emerges from Ohmic current contact 2 and propagates dissipationlessly along the edge of the central segment A toward contact 3. μ_3 adjusts so that total current emerging from contact 3 equals the edge current arriving from 2. A shift in μ_3 causes both edge and bulk currents to emerge from contact 3, so that edge current emerging from contact 3 is less than edge current entering it. The bulk current emerging from contact 3 returns through the central segment to contact 6; no net current is passed through 3, 4, or 5. The same considerations apply for contacts 4 and 5 as for 3. Edge current emerging from 3 is therefore further attenuated at 4 and 5; μ_4 and μ_5 are correspondingly shifted by smaller amounts than μ_3. A potential difference results between voltage contacts 3 and 5, i.e., nonzero R_{NL}. In the case $\rho=0$ in Eq. (1), however, corresponding to $\nu=i+1$, bulk current is indistinguishable from edge current (in this model) and potential differences are zero except across current contacts 2 and 6. In the limit of $\rho\rightarrow\infty$, corresponding to $\nu=i$, bulk current does not flow and only edge current circulates. Only for finite, positive ρ do dissipative bulk currents contribute to nonzero nonlocal potential differences, between contacts far from the sample area directly between current contacts.

2DES transport in the IQHE regime can also be treated in the more general language of many-electron wave functions which allows one to include electron-electron interaction. For ν between integers i and $i+1$, the 2DES state can be regarded as comprised of the IQHE state at i, extending from edge to edge, plus the quasiparticles [electrons in the $(i+1)$st Landau level] needed to produce the given ν in the 2DES interior. This picture generalizes straightforwardly to 2DES states in the FQHE regime.[14] The quantitative model[4] of FTMR's in the IQHE can then be extended to the FQHE for ν between rational fractions p/q and p'/q' $(p/q<p'/q')$ corresponding to FQHE states with no other QHE states between.[17] In Eq. (2) we set $N_E=p/q$ and $N_B=(p'/q')-(p/q)$. That is, on emerging from contacts, the edge current passes through contact resistance $(q/p)(h/e^2)$, and the bulk current passes through contact resistance $(h/e^2)[(p'/q')-(p/q)]^{-1}$. As in the IQHE, bulk dissipation is modeled in terms of partial reflection of the bulk current while circulating around the Hall bar. T_j is again parametrized by Eq. (1) for bulk current flowing through a lead region between contact j and the central segment, in terms of a bulk resistivity ρ. Modifying N_E and N_B above in Eq. (2) may appear arbitrary. This generalization of the model of Ref. 4 generates correct FTMR's, however, in the case $\rho=0$, for an FQHE state at $\nu=p'/q'$. That is, $R_{NL}=0$, $R_{xx}=0$, and Hall resistance R_{xy} equals contact resistance, $(q'/p')(h/e^2)$. In the case of large ρ, FTMR's also approach correct values for an FQHE state at $\nu=p/q$. As ρ varies between 0 and infinity, peaks occur in R_{xx} and R_{NL}, while R_{xy} varies between $(q/p)(h/e^2)$ and $(q'/p')(h/e^2)$, consistent with experiment.

III. EXPERIMENT

A. Materials and measurements

2DES samples were prepared from low-disorder GaAs/$Al_{1-x}Ga_xAs$ heterojunction material. Standard, simply connected Hall bar patterns, such as shown in Fig. 2(b), were defined in some samples by wet etching. Patterns were defined with varying length-to-width ratios both of the Hall bar central segment [L_A/W_A in Fig. 2(a)] and of the lead regions (L_j/W_j). Ratios L_A/W_A ranged between 1 and 20; widths of central segments and lead regions were 10–120 μm within overall pattern size $\sim$1 mm. In Fig. 2(b), $L_A/W_A\approx 2.2$, and $L_j/W_j\approx 5$–7 for the lead regions connecting to contacts 2, 3, 5, and 6. Rectangular samples were also tested, as in Fig. 2(c),

without distinct lead regions to the Ohmic contacts made at the edges.

Brief illumination with a red light-emitting diode was used to prepare 2DES with density $(7-12)\times10^{10}$ cm^{-2} and mobility $(6-20)\times10^{5}$ cm^2/V s. FTMR's were measured using standard low-frequency lock-in technique, with ac measurement currents between 0.1 and 10 nA. In Hall bar samples with lead regions [Fig. 2(b)], R_{xx} was measured as $R_{14,23}$ and $R_{14,56}$; R_{xy} was measured as $R_{14,26}$ and $R_{14,35}$; and $R_{\rm NL}$ was measured as $R_{26,35}$ and $R_{35,26}$. In rectangular samples [Fig. 2(c)], R_{xx} was measured as $R_{12,34}$ and $R_{34,12}$; and $R_{\rm NL}$ was measured as $R_{13,24}$ and $R_{24,13}$.

B. Role of sample geometry in magnetoresistance measurements

Figure 3 shows $R_{xx}(B)$, $R_{xy}(B)$, and $R_{\rm NL}(B)$ for one sample, etched with the Hall bar pattern in Fig. 2(b), at 20 mK. The sample also displays FQHE at $\nu=\frac{1}{5}$ at higher B, not shown. $R_{\rm NL}$ is magnified by a factor of 3 relative to R_{xx} in Fig. 3. Examination of Fig. 3 immediately reveals drastic differences between $R_{xx}(B)$ and $R_{\rm NL}(B)$. For classical, dissipative, homogeneous (without edge states) 2DES transport in a Hall bar geometry, $R_{\rm NL}(B)$ is the same as $R_{xx}(B)$ except for being reduced by a *B-independent* geometric factor.[18] The factor should be $\sim10^{-3}$ for $L_A/W_A=2.2$, consistent with $R_{\rm NL}=1.3\times10^{-3}R_{xx}$ measured at $B=0$. In Fig. 3, however, as a function of B, $R_{\rm NL}$ exhibits peaks with heights on the order of 10^{-1} (or larger) of R_{xx} at the same B. Over some intervals of B, particularly near $\nu=\frac{1}{2}$ and on the low ν side of $\nu=1$, $R_{\rm NL}$ differs negligibly from zero, while R_{xx} is prominently nonzero. At B between certain pairs of FQHE states, (e.g., between $\frac{1}{3}$ and $\frac{2}{5}$, and between $\frac{2}{5}$ and $\frac{3}{7}$) R_{xx} and $R_{\rm NL}$ exhibit corresponding peaks. These peaks generally differ, however, in their positions and shape. Ratios of corresponding peak heights in R_{xx} and $R_{\rm NL}$ also vary greatly for different peaks. Clearly, measurements of $R_{\rm NL}(B)$ and $R_{xx}(B)$ at 20 mK characterize essentially different properties of 2DES transport in the FQHE regime.

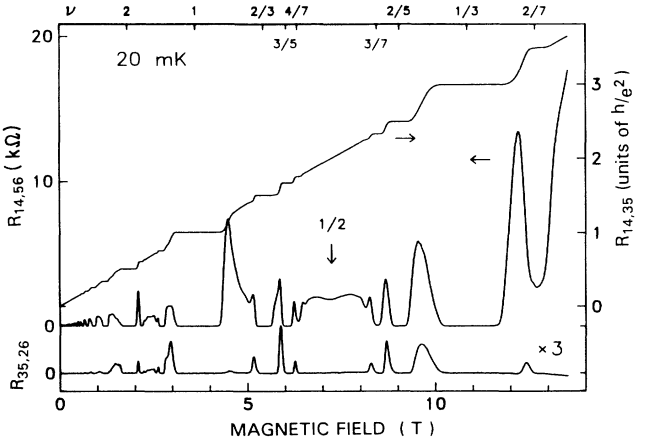

FIG. 3. Longitudinal ($R_{14,56}$), Hall ($R_{14,35}$), and "nonlocal" ($R_{35,26}$) four-terminal magnetoresistances (FTMR) of a sample etched with the Hall bar pattern of Fig. 2(b) at 20 mK. ν is labeled along the top of the frame. While nonzero longitudinal FTMR (R_{xx}) implies dissipative transport, nonzero nonlocal FTMR ($R_{\rm NL}$) implies transport by *both* dissipative bulk and decoupled edge currents at that ν. Note the qualitatively different shapes of R_{xx} and $R_{\rm NL}$. $R_{\rm NL}$ is magnified by a factor of 3 compared to R_{xx}.

FTMR's were also measured for rectangular samples with $L/W>2$. $R_{xx}(B)$ for these samples is similar to $R_{xx}(B)$ for Hall bar patterns; however, $R_{\rm NL}(B)\approx0$ (not shown). Nonzero nonlocal FTMR evidently occurs only in Hall bars with distinct lead regions, as in Figs. 2(a) and 2(b). In Hall bar samples defined with $L_A/W_A<2$ (short central segments), $R_{\rm NL}(B)$ was appreciably mixed with an $R_{xx}(B)$ component. This is expected for samples approximating a square van der Pauw geometry[18] ($L_A/W_A\approx1$). In consideration of these results, we conducted further studies of nonlocal FTMR's using only Hall bar samples with distinct lead regions and $L_A/W_A\geq2$.

For a given Hall bar geometry, FTMR's in different measurement configurations exhibit certain global symmetry relations. Figures 4(a) and 4(b) show $R_{\rm NL}(B)$ measured as $R_{26,35}$ and $R_{35,26}$, respectively, i.e., in two configurations differing by switching pairs of current and voltage contacts. Each FTMR is shown for B in both directions (perpendicular to the 2DES plane); these data are labeled $B+$ and $B-$. Data are from the sample of Fig. 3; $B+$ is defined pointing into the Hall bar plane (Fig. 2). Figures 5(a) and 5(b) show $R_{xx}(B)$ for another sample in the QHE regime, measured as $R_{14,65}$ and $R_{14,23}$, respectively, i.e., in two configurations with the pair of voltage contacts on opposite sides of the same pair of current contacts. In Fig. 5 each FTMR is plotted with B in both directions, as in Fig. 4. We now compare traces taken with B in the same direction, either $B+$ or $B-$. Various features in any two traces have unequal

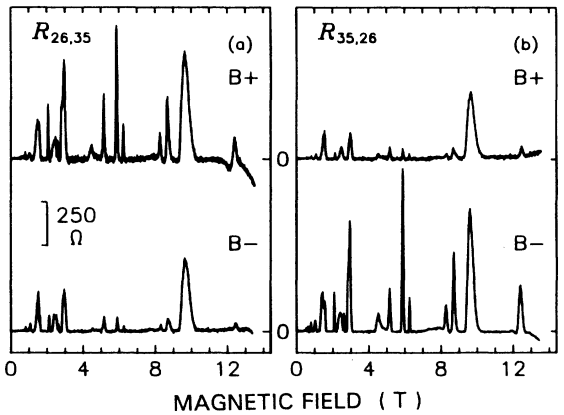

FIG. 4. $R_{\rm NL}(B)$ measured as (a) $R_{26,35}$ and (b) $R_{35,26}$, for the sample of Fig. 3 at $\sim$20 mK. Each FTMR is shown for B in both directions perpendicular to the 2DES plane labeled $B+$ and $B-$. $B+$ is defined pointing into the Hall bar plane in Fig. 2(b).

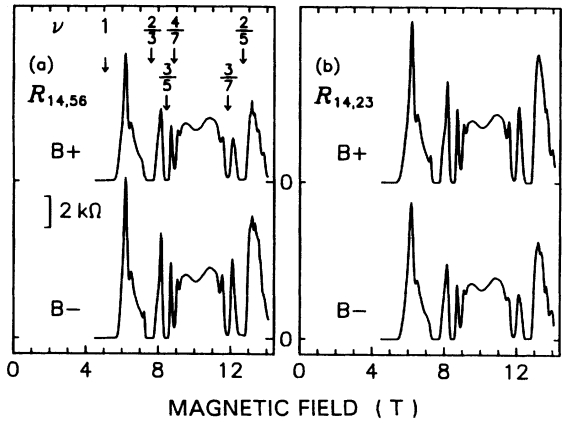

FIG. 5. $R_{xx}(B)$ measured as (a) $R_{14,65}$ and (b) $R_{14,23}$ for another sample at ~20 mK. Each FTMR is shown for B in both directions as in Fig. 4.

size and/or shape versus B. In Figs. 4(a) and 4(b), for example, R_{NL} peaks for $B+$ are generally larger in $R_{26,35}$ than in $R_{35,26}$. In Figs. 5(a) and 5(b), R_{xx} peaks for $B+$ are generally more pronounced in $R_{14,23}$ than in $R_{14,65}$. These size and shape differences are reversed upon reversal of the direction of B and are not affected by the presence and direction of I_{dc} superimposed on the ac current used to measure resistance. Apparently, a nonzero FTMR depends on the coexisting and decoupled bulk and edge conduction throughout a Hall bar. In $R_{14,65}$, for example, heights of peaks and depths of minima do not simply depend on a bulk resistivity in the central segment. Upon reversal of B, which reverses the direction of edge currents, features of peaks and minima in $R_{14,65}$ are changed, while $R_{14,23}$ exhibits the same features observed in $R_{14,65}$ with the original B direction. The differences between $R_{14,23}$ and $R_{14,65}$, or between $R_{36,25}$ and $R_{25,36}$, apparently originate in the differences in detailed shape of the lead regions [Fig. 2(b)].

C. Effects of variation of temperature, current and sweep direction

In order to elucidate the processes generating nonlocal resistances in FQHE transport, we measured FTMR's as a function of T and of I_{dc}. In Fig. 6(a) we show $R_{NL}(B)$ at several different T. Figure 6(b) shows R_{xx} at 320 mK. From the data of Fig. 6, along with R_{xx} at 20 mK in Fig. 3, it is clear that as T is increased up to 350 mK, R_{NL} peaks all diminish considerably, while the magnitude of R_{xx} generally decreases little.

We also obtained a detailed T dependence of R_{NL} peaks by varying T at a fixed B, for one peak at a time. Figure 7 shows R_{NL} at $B=9.62$ T ($\nu=0.38$), on the peak between $\frac{1}{3}$ and $\frac{2}{5}$, as a function of T. $R_{NL}(\nu=0.38)$ decreases monotonically with increasing T and approaches a finite value, ≈ 0.76 kΩ, in the limit of zero T. This T dependence was reproducible with T swept increasing or decreasing.

In Fig. 8 we plot the dependences of R_{NL} and R_{xx} on applied I_{dc} between −70 nA and +70 nA, superimposed

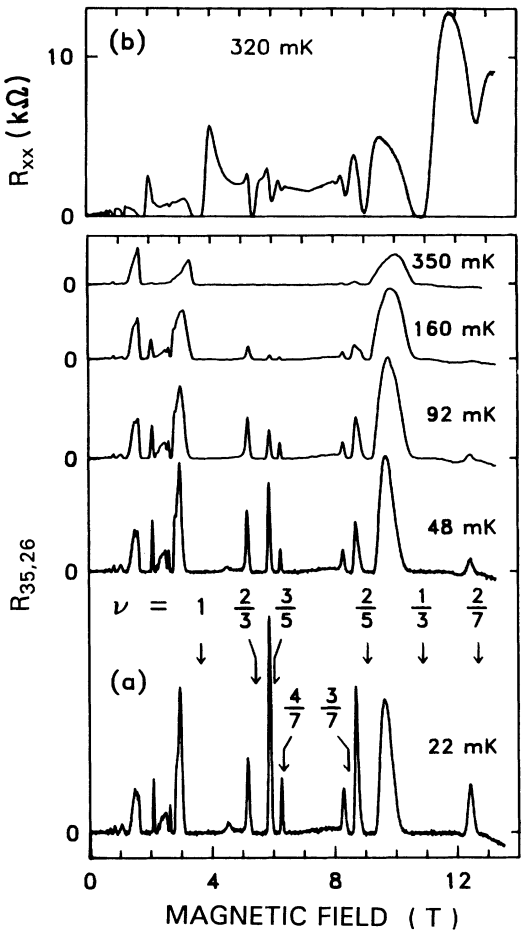

FIG. 6. (a) R_{NL} at different values of T, for the sample of Fig. 3. All traces in (a) have the same scale of resistance. The origin of the weak peak at 4.5 T is not known at present; its disappearance by 60 mK seems to rule out the $\nu=1$ IQHE state. (b) R_{xx} at 320 mK.

upon ac measurement current I_{ac} (1 nA) at $T=27$ mK. As in Fig. 7, $B=9.62$ T ($\nu=0.38$), on the R_{NL} peak between $\frac{1}{3}$ and $\frac{2}{5}$. I_{dc} was ramped over 2 h for each sweep; peak heights were completely reproducible over this time span. At a fixed B, R_{NL} [Fig. 8(a)] decreases much more sharply than R_{xx} [Fig. 8(b)] versus I_{dc}, for both direc-

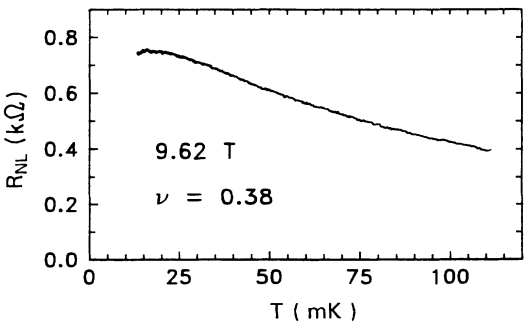

FIG. 7. R_{NL} at fixed $B=9.62$ T ($\nu=0.38$) vs T.

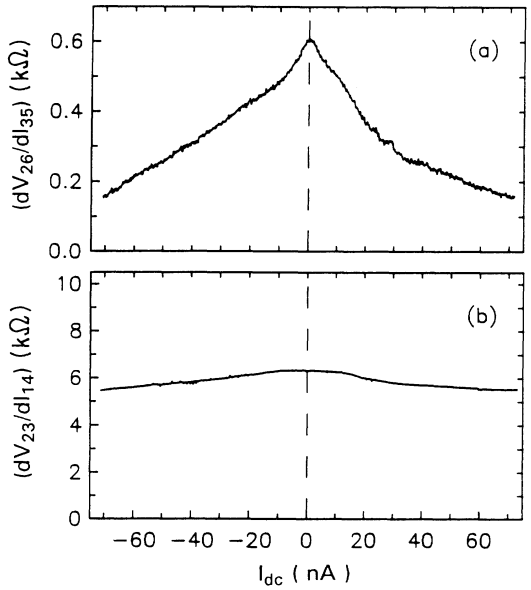

FIG. 8. (a) $R_{NL}(dV_{26}/dI_{35})$ vs I_{dc}; and (b) $R_{xx}(dV_{23}/dI_{14})$ vs I_{dc} for the sample of Fig. 3. For both traces $B=9.62$ T ($\nu=0.38$), $T=27$ mK, and ac measurement current $I_{ac}=1$ nA rms.

tions of I_{dc}. That is, at $\nu=0.38$ R_{NL} becomes appreciably nonlinear versus I_{dc} at much smaller values of I_{dc} (~ 5 nA) than R_{xx} (at >70 nA). In sweeps of R_{NL} versus B, the size and shape of $R_{NL}(B)$ peaks were similar at 20 mK with applied $I_{dc}=20$ nA, and at about 150 mK with zero I_{dc}. This similarity suggests that increasing T or I_{dc} attenuates nonlocal potential differences by similar processes; i.e., the primary effect of higher currents on nonlocal FTMR is Joule heating.

We observe that $R_{NL}(B)$ peak heights in the FQHE regime are unusually sensitive to the finite sweep rate of B. Also, this sensitivity is asymmetric so that $R_{NL}(B)$ peak heights are different in the sweeps up than in sweeps down for the same (in magnitude) sweep rates of about 1×10^{-3} T/s. In Fig. 9 we show two traces of $R_{NL}(B)$ obtained sweeping B up and down at a rate of 5×10^{-4} T/s. At much lower sweep rates $R_{NL}(B)$ approaches a limiting value; we check this by stopping the sweep. This sweep rate sensitivity and the polarity-dependent difference, not completely understood at present, are most prominent at $T<50$ mK and are completely reproducible over periods of several days. The data of Figs. 3–8 were obtained with sweep rates slow enough and are believed to be in the $dB/dt\rightarrow0$ limit. $R_{xx}(B)$ does not vary noticeably with sweep rate or direction.

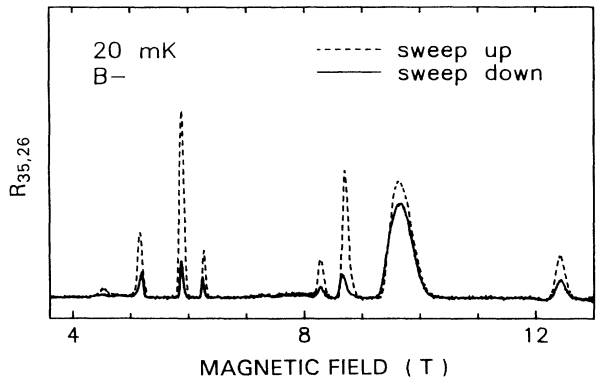

FIG. 9. R_{NL} at about 20 mK with B swept up and down at a rate of 5×10^{-4} T/s.

IV. ANALYSIS AND DISCUSSION

In the FQHE regime we have observed R_{NL} and R_{xx} of comparable magnitude but strikingly different dependences on B, T, and I_{dc} (Figs. 3–8). These differences imply the existence of simultaneous dissipative bulk conduction and dissipationless edge conduction in a 2DES Hall bar, and resulting nonlocal potential differences which extend throughout the Hall bar pattern. Results differ dramatically, however, for FTMR measurements in different Hall bar patterns. Apparently, R_{NL} can be measured only in certain sample geometries, specifically, when L_A/W_A is of intermediate size, 2–10, and $L_j/W_j>L_A/W_A$. These conditions can be explained in terms of geometric considerations, within the model of coexisting bulk and edge conduction discussed in Sec. II. Some degree of R_{xx} mixing in R_{NL} is always expected due solely to bulk conduction;[18] this mixing obscures nonlocal transport effects if $L_A/W_A<2$. If L_j/W_j is small relative to L_A/W_A, then different potentials in the Hall bar will adjust so that μ_2, μ_6, and μ_1 all differ little from μ_A (Fig. 2). The difference $\mu_6-\mu_2$, i.e., $R_{35,26}$, will then be reduced, consistent with our experimental results. Nonlocal transport thus involves all components of a Hall bar pattern, including Ohmic contacts and lead regions.

The global symmetry properties demonstrated in Figs. 4 and 5 confirm that, strictly speaking, all FTMR's are nonlocal in the FQHE. The observed properties are similar to (for R_{NL}, identical to) Onsager-Casimir (OC) symmetry relations for irreversible processes.[19] Büttiker[20] has shown that four-terminal conductance in samples also satisfies OC relations, assuming that currents scatter elastically within the sample and equilibrate irreversibly in Ohmic contact reservoirs. These assumptions are implicitly made in the model of Sec. II, since Eq. (1) relates dissipation of bulk current to transmission coefficients T_j between dissipationless channels. Using this model we have calculated R_{xx} and R_{NL}, in different 4-lead configurations, for edge currents circulating in both directions between contacts (not shown). Consistent with Ref. 20, the OC relation observed for R_{NL} (Fig. 4) is satisfied by calculations for Hall bar geometries with some of the leads of unequal L_j/W_j. The symmetry relation observed for R_{xx} (Fig. 5) is not generally satisfied in calculations with arbitrary L_j/W_j. The R_{xx} symmetry relation is satisfied only for Hall bars bilaterally symmetric about contacts 1 and 4, i.e., with $L_2/W_2=L_6/W_6$ and $L_3/W_3=L_5/W_5$. We note that the Hall bar pattern in Fig. 2(b) very nearly satisfies this bilateral symmetry,

with lead regions 2 and 6 somewhat longer than 3 and 5. Nonlocal transport in the FQHE apparently can be well understood in terms of edge conduction in one direction around the sample perimeter; the direction is reversed upon reversal of B (Figs. 4 and 5).

In Fig. 10 continuous traces show R_{xx} and $R_{\rm NL}$, plotted versus R_{xy}. Each of Figs. 10(a)–10(c) plots a different interval of R_{xy}, with R_{xx} plotted in the upper frame and $R_{\rm NL}$ in the lower frame. Data were obtained at 20 mK. Dotted lines show calculations of the same FTMR's for the Hall bar geometry shown in Fig. 2(b) using the bulk-edge model extended to the FQHE regime (Sec. II). Plotted in this way, results of calculations are independent of parameter ρ. In Fig. 10(c), calculation for $\frac{4}{7}>\nu>\frac{4}{9}$ (around $\frac{1}{2}$) is not plotted for R_{xx} nor for $R_{\rm NL}$. We also do not model $R_{\rm NL}$ for $1>\nu>\frac{5}{7}$, and between $\frac{1}{3}$ and $\frac{2}{7}$. Measured $R_{\rm NL}$ is zero over parts of the interval of ν in each of these cases; these intervals do not correspond to expected sequences of transitions between FQHE states.[17] In Fig. 10(b) calculations are not shown for the interval $\frac{8}{5}>\nu>\frac{7}{5}$, near $\nu=\frac{3}{2}$; edge-channel structure in this interval is more complicated for this interval of ν since edge channels extending from the $\nu=1$ IQHE state must emerge for some ν near $\frac{3}{2}$ in this interval.[14,17]

Agreement between the data and calculations shown in Figs. 10(a)–10(c) varies for different FTMR peaks in different intervals of R_{xy}. The peak heights in calculations and data all agree within order of magnitude. Calculated peak heights in R_{xx} ($R_{\rm NL}$) are in general smaller (larger) than in the data. One qualitative feature of the data is systematically reproduced in calculations: peak maxima are at higher ν (lower R_{xy}) in R_{xx} than in $R_{\rm NL}$. That is, R_{xx} peaks "lean" more towards lower R_{xy} than $R_{\rm NL}$ peaks do, in both the data and calculations in Figs. 10(a)–10(c).[21] The present model seems to incorporate correctly some basic physics of bulk-edge transport in the FQHE regime. Agreement with data could be improved much with minor modifications of the model. For example, the bulk channel transmission coefficients T_j and T_A might be parametrized by some expression other than Eq. (1), with the condition that coefficients equal 0 or 1 at ν corresponding to QHE states. Transmission coefficients T_j' and T_A' might also be introduced for the edge channels. Such coefficients would parametrize scattering between edge and bulk states and would, presumably, not deviate greatly from unity when nonlocal conduction is observed. Another modification, N_B in Eq. (2), might be treated as a variable of ρ. To model FTMR's between p/q and p'/q', one would require only that $N_B(\rho=0)=[(p'/q')-(p/q)]$. At present, however, none of these modifications is specifically suggested by our data or by a fundamental theory of FQHE transport. They therefore do not seem to be warranted complications of the present model.

A possible physical origin of the T dependence is phonon-assisted scattering between bulk and edge currents within the sample. Bulk-edge scattering processes were originally neglected in applications of the bulk-edge model in the IQHE regime.[4] Processes involving scattering from one edge to the bulk, followed by scattering to the opposite edge are, equivalently, back-scattering between edge channels. Such scattering, edge-bulk-edge or edge-bulk, would attenuate an edge current that emerged from an Ohmic contact before the edge current reached another contact, and would thus reduce nonlocal potential differences ($R_{\rm NL}$). R_{xx} magnitude is less sensitive to any bulk-edge mixing within a 2DES sample. We conclude that the disappearance of $R_{\rm NL}$ peaks at higher T is due primarily to scattering between edge and bulk currents, along distances of ~ 1 mm in the 2DES sample. Scattering probability increases as T is raised, while R_{xx} peaks are not significantly affected, con-

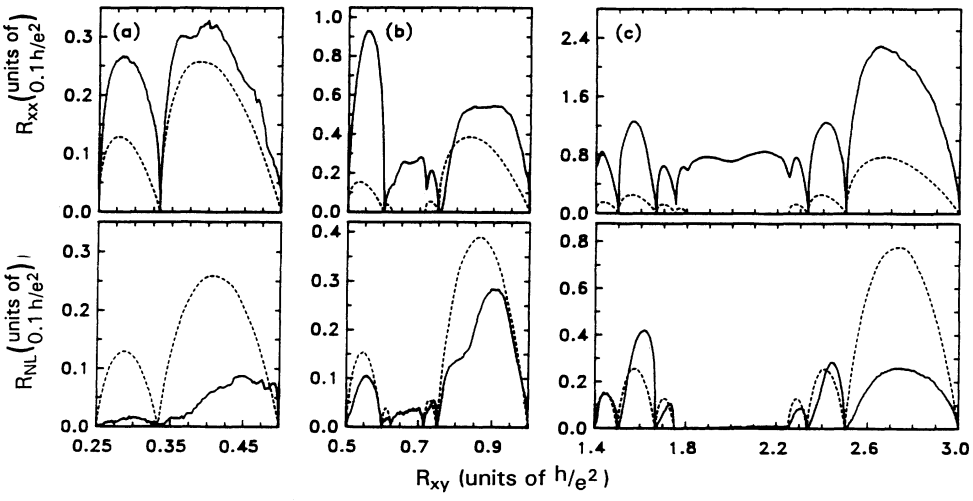

FIG. 10. R_{xx} and $R_{\rm NL}$ vs R_{xy} calculated using the model described in Sec. II for the Hall bar geometry at Fig. 2(b) (dashed lines). Continuous traces are the data at 20 mK (Fig. 3). Plots are over different intervals of R_{xy} (in units of h/e^2): (a) between $\frac{1}{4}$ and $\frac{1}{2}$; (b) $\frac{1}{2}$ and 1 (no calculation for $\frac{8}{5}>\nu>\frac{7}{5}$); and (c) $\frac{7}{5}$ and 3 (no calculation for $\frac{4}{7}>\nu>\frac{4}{9}$). In each of (a)–(c), R_{xx} is plotted in the upper frame and $R_{\rm NL}$ in the lower frame.

sistent with our experimental observations.

R_{NL} and R_{xx} magnitudes are calculated in the present model in the zero T limit. In Fig. 6(a), measured R_{NL} peak heights in the IQHE regime (0–2 T) vary little for $T<200$ mK, consistent with data of McEuen *et al.*[4] In Ref. 4, R_{NL} peak heights do not diminish for T up to 1 K, presumably because the IQHE regime extends to 10 T in their data. At higher B Landau levels are separated by larger energy gaps ($\sim B$); the model assumption, that edge and bulk currents do not interscatter within the 2DES, is then better satisfied at higher B.

It is noteworthy that scattering is largely suppressed over macroscopic distances for FQHE edge currents even though excitation gaps of FQHE states are appreciably smaller than the gaps of IQHE states so that bulk-edge separation would appear to be much smaller in the FQHE regime. In Fig. 6(a), in the FQHE regime, R_{NL} peaks decrease significantly versus increasing T. Different T dependences are observed for different R_{NL} peaks. We have proposed[14] that survival to higher T of a given R_{NL} peak is correlated with greater stability, i.e., larger excitation gap, for the supporting FQHE state. With this ansatz we observed that an FQHE state at ν_0 supports R_{NL} peaks only at ν greater than ν_0 [Fig.6(a)]. Electron-hole symmetry is thus broken for bulk and edge states in a confined geometry.[14]

We have observed (Fig. 7) that, as a function of T, $R_{NL}(\nu=0.38)$ approaches a finite value in the limit of zero T. This asymptotic behavior is more obvious in the plot of $R_{NL}(\nu=0.38)$ versus T^{-1}, shown in Fig. 11. Small solid circles at higher T mark points taken from sweeps of B at a fixed T. We have fitted $R_{NL}(\nu=0.38)$ versus T with several simple analytic expressions; we find close fits of the form

$$R_{NL}=\alpha\{\beta T/[\exp(\beta T)-1]\}\ , \tag{3}$$

in terms of only two parameters. Each parameter has clear physical interpretation: α is an overall geometry-dependent constant, equal to R_{NL} at zero T; β^{-1} gives the activation energy. In Fig. 11, solid squares represent an optimal fit[22] using Eq. (3) with $\alpha=0.85$ kΩ and $\beta=(80\ \text{mK})^{-1}$. This value of β^{-1} is much smaller than either of the activation energies at $\nu=\frac{2}{5}$ and $\nu=\frac{1}{3}$ (the gaps for these FQHE states). This and the fact that R_{NL} disappears at much lower T than R_{xx} at the same ν leads us to believe that increased edge-bulk scattering is responsible for disappearance of R_{NL} as T is raised.

We have attributed the decrease of R_{NL} with increasing current (Fig. 8) to Joule heating effects which effectively raise the 2DES T (Sec. III C). Calculations by Wen[11] indicate, however, that tunneling between FQHE edges generally depends nonlinearly on the potential difference $\Delta\mu$ between the channels, with a power-law dependence on small $\Delta\mu$. It is possible that this intrinsically nonlinear bulk-edge tunneling contributes to the nonlinear current dependence of R_{NL}. For very small currents, $\Delta\mu$ is nearly proportional to current. Joule heating then results in $\delta R_{NL}/R_{NL}\sim I^2\sim(\Delta\mu)^2$, and would dominate effects with higher power-law dependence. We do not attempt more detailed analysis of the effects of heating and intrinsic nonlinear conductance, given the present limited understanding of either effect in FQHE transport.

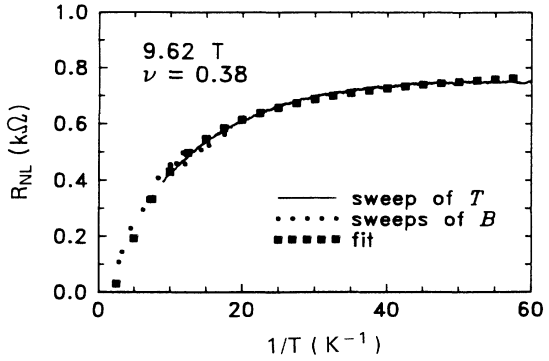

FIG. 11. R_{NL} at $B=9.62$ T ($\nu=0.38$) plotted vs T^{-1}. Continuous line is the data of Fig. 7, dots at higher T show points obtained from sweeps of B at fixed T (cf. Fig. 6). Solid squares give the best fit by Eq. (3) with $\alpha=850\ \Omega$, $\beta=(80\ \text{mk})^{-1}$.

As developed thus far, our picture of conduction in the FQHE regime does not explain the dependence of R_{NL} on B sweep rate, dB/dt, and the asymmetry with respect to dB/dt polarity (Fig. 9). This rate dependence suggests a mechanism involving eddy currents around the sample perimeter, due to emf induced by varying B within the perimeter. In a typical experiment, $|dB/dt|\sim 8$ G/s; this induces ~ 1 nV dc emf around the perimeter of a ~ 1 mm^2 sample area. This emf could generate significant current within edge channels, across small channel resistances due to perturbatively small scattering processes. If an edge channel has resistance 0.03 Ω, for example, then 1 nV induced by sweeping B would generate 30 nA dc in that channel. When B sweep direction is reversed, eddy current direction is also reversed. In Fig. 8(a), R_{NL} is asymmetric with respect to the polarity of I_{dc} and is reduced 50% by $I_{dc}\approx 30$ nA. Eddy currents may act effectively as I_{dc}, causing nonlinear effects in nonlocal transport, which we have suggested are due to current heating and/or nonlinear tunneling conductance between different channels.[11] We repeat that dependence of R_{NL} on dB/dt rate and the asymmetry with respect to dB/dt polarity are not fully understood at present.

V. CONCLUSIONS

We have previously reported[14] nonlocal FTMR as a useful probe of bulk and edge-state conduction in the FQHE regime. We present here a more detailed experimental study of longitudinal and nonlocal FTMR's in the FQHE regime. We deduce from the data that FTMR's in the FQHE, as in the IQHE,[4] are *all* nonlocal, determined by conduction throughout a sample. I_{dc} and T dependence of FTMR's gives evidence for bulk and edge current interscattering in the 2DES. We report large

anomalous dependence of nonlocal FTMR on B-sweep rate and direction; we suggest this is due to dB/dt-induced eddy currents in edge channels. In summary, transport in the FQHE is a complex, nonlocal phenomenon. Dissipationless edge currents and dissipative bulk currents interact via different mechanisms, with significant dependence on the 2DES geometry and Ohmic contacts.

ACKNOWLEDGMENTS

We are grateful to J. K. Jain for interesting and stimulating discussions and to M. Shayegan and J. E. Cunningham for expertly grown molecular-beam-epitaxy heterostructure material. This work was supported in part by the NSF under Grants No. DMR-8958453 and No. DMR-9013053.

[1]K. von Klitzing, G. Dorda, and M. Pepper, Phys. Rev. Lett. **45**, 494 (1980); for a review, see *The Quantum Hall Effect,* edited by R. E. Prange and S. M. Girvin (Springer-Verlag, New York, 1987).

[2]R. B. Laughlin, Phys. Rev. B **23**, 5632 (1981); B. I. Halperin, *ibid.* **25**, 2185 (1982); S. A. Trugman, *ibid.* **27**, 7539 (1983); A. H. MacDonald and P. Streda, *ibid.* **29**, 1616 (1984); J. K. Jain and S. A. Kivelson, Phys. Rev. Lett. **60**, 1542 (1988); M. Büttiker, Phys. Rev. B **38**, 9375 (1988).

[3]K. von Klitzing *et al.*, *Proceedings of the 17th International Conference on the Physics of Semiconductors* (Springer-Verlag, New York, 1985), p. 271; H. Z. Zheng, K. K.Choi, D. C. Tsui, and G. Weigman, Phys. Rev. Lett. **55**, 1144 (1985); B. E. Kane, D. C. Tsui, and G. Weigman, *ibid.* **59**, 1353 (1987); R. J. Haug, A. H. MacDonald, P. Streda, and K. von Klitzing, *ibid.* **61**, 2801 (1988); B. J. van Wees *et al.*, *ibid.* **62**, 1181 (1989).

[4]P. L. McEuen *et al.*, Phys. Rev. Lett. **64**, 2062 (1990); A. Szafer *et al.* (unpublished). McEuen *et al.* demonstrate that *all* FTMR's are, strictly speaking, nonlocal. We use terminology "nonlocal FTMR" to denote the most dramatically nonlocal FTMR, as opposed to R_{xx} and R_{xy}.

[5]D. C. Tsui, H. L. Stormer, and A. C. Gossard, Phys. Rev. Lett. **48**, 1559 (1982).

[6]R. B. Laughlin, Phys. Rev. Lett. **50**, 1395 (1983).

[7]F. D. M. Haldane, Phys. Rev. Lett. **51**, 605 (1983); B. I. Halperin, *ibid.* **52**, 1583 (1984).

[8]J. K. Jain, Phys. Rev. Lett. **63**, 199 (1989); Phys. Rev. B **41**, 7653 (1990); J. K. Jain and V. J. Goldman, *ibid.* **45**, 1255 (1992).

[9]C. W. J. Beenakker, Phys. Rev. Lett. **64**, 216 (1990).

[10]A. H. MacDonald, Phys. Rev. Lett. **64**, 220 (1990); M. D. Johnson and A. H. MacDonald, *ibid.* **67**, 2060 (1991).

[11]X. G. Wen, Phys. Rev. Lett. **64**, 2206 (1990); Phys. Rev. B **44**, 5708 (1991).

[12]A. M. Chang and J. E. Cunningham, Surf. Sci. **229**, 216 (1990); Solid State Commun. **72**, 651 (1989).

[13]L. P. Kouwenhoven *et al.*, Phys. Rev. Lett. **64**, 685 (1990).

[14]J. K. Wang and V. J. Goldman, Phys. Rev. Lett. **67**, 749 (1991).

[15]It has been shown that fully occupied Landau levels are equilibrated, even on a very short length scale, and therefore can be considered all together; B. W. Alphenaar, P. L. McEuen, R. G. Wheeler, and R. N. Sacks, Phys. Rev. Lett. **64**, 677 (1990).

[16]J. K. Jain and S. A. Kivelson (Ref. 2).

[17]It can be argued that such extension of an IQHE model to the FQHE regime is appropriate only for the sequences of transitions between FQHE states analogous to the IQHE sequence. See J. K. Jain, S. A. Kivelson, and N. Trivedi, Phys. Rev. Lett. **64**, 1297 (1990); V. J. Goldman, J. K. Jain, and M. Shayegan, Mod. Phys. Lett. **5**, 479 (1991).

[18]L. J. van der Pauw, Philips Res. Rep. **13**, 1 (1958).

[19]L. Onsager, Phys. Rev. **38**, 2265 (1931); H. B. G. Casimir, Rev. Mod. Phys. **17**, 343 (1945).

[20]M. Büttiker, Phys. Rev. Lett. **57**, 1761 (1986); also, M. Büttiker (Ref. 2).

[21]Positions of the longitudinal resistance peaks have been measured accurately in V. J. Goldman, J. K. Jain, and M. Shayegan, Phys. Rev. Lett. **64**, 1297 (1990). Here we comment that these positions, in general, are affected by the sample geometry [this result for IQHE was obtained by H. Z. Zheng *et al.* (Ref. 3)]; however, for leadless, large, rectangular samples with $L/W \sim 1$ these posistions are not sensitive to the exact sample geometry.

[22]In the limit of low T, Eq. (3) deviates from $\alpha = 0.85$ kΩ as $\alpha(1-\frac{1}{2}\beta T)$, a linear dependence on T. The data in Fig. 11, however, seem to approach a lower limit at zero T, $\alpha \approx 0.76$ kΩ, and with a stronger T dependence, perhaps as $[1-(\beta T)^{\gamma}]$, where $\gamma \gg 1$, or as $[1-\exp(-1/\beta T)]$.